RESEARCH ARTICLE

Blood Science

OPEN

Super-resolution imaging informed scRNA sequencing analysis reveals the critical role of GDF15 in rejuvenating aged hematopoietic stem cells

Zhongyu Shi[a], Xuefei Zhang[b], Huihui Yang[a], Xiaolu Zheng[b], Mengxiao Niu[b], Yongjian Zhang[a], Pengfei Yuan[a], Wensheng Wei[c,d], Gang Huang[e,*], Riguo Fang[a,f,*], Liangyi Chen[b,g,h,*]

[a]EdiGene Inc., Beijing, China; [b]New Cornerstone Science Laboratory, National Biomedical Imaging Center, State Key Laboratory of Membrane Biology, Beijing Key Laboratory of Cardiometabolic Molecular Medicine, Institute of Molecular Medicine, School of Future Technology, Center for Life Sciences, Peking University, Beijing 100871, China; [c]Biomedical Pioneering Innovation Center, Peking-Tsinghua Center for Life Sciences, Peking University Genome Editing Research Center, State Key Laboratory of Protein and Plant Gene Research, School of Life Sciences, Peking University, Beijing 100871, China; [d]Changping Laboratory, Beijing, China; [e]Departments of Cell Systems and Anatomy/Pathology and Laboratory Medicine, UT Health San Antonio, Joe R. and Teresa Lozano Long School of Medicine, 8403 Floyd Curl Drive, San Antonio, TX 78229; [f]EdiGene (Guangzhou) Inc., Guangzhou, China; [g]National Biomedical Imaging Center, Beijing 100871, China; [h]PKU-IDG/McGovern Institute for Brain Research, Beijing 100871, China

Abstract

Although changes in mitochondrial morphology consistently associated with the aging of hematopoietic stem cells (HSCs), the specific molecular and cellular mechanisms involved are partially unclear. Live-cell super-resolution (SR) microscopy has been used to identify distinct HSC subsets that characterized by mitochondria unique morphologies and spatial distributions. The integration of SR microscopy with single-cell RNA sequencing enabled the classification of approximately 200 HSCs from young and aged mice into 5 discrete clusters. These clusters displayed molecular profiles that corresponded to the observed mitochondria states. An integrated approach combining RNA biomarker analysis and potential regulon assessment revealed previously unrecognized roles of GDF15 in mediating mitochondrial signals and morphologies that influence HSC fate. Thus, combining SR imaging with a bioinformatics pipeline provides an effective method for identifying key molecular players in specific phases of cellular transition, even with a relatively small dataset.

Key Words: Hematopoietic stem cells; Mitochondria; scRNA sequencing; Super-resolution microscopy

1. INTRODUCTION

Mitochondria are essential organelles for oxidative phosphorylation, energy production, and the synthesis of many metabolites.[1] These organelles form a dynamic network within living cells and extensively interact with other cellular compartments. Through these interactions, mitochondria mediate numerous cellular signaling processes and influence cell fate changes relevant to aging and age-related diseases, such as cancer,[2] neurological disorders,[3] and metabolic diseases,[4,5] among others.[6] Although many types of stem cells are deficient in mitochondria[7] and are thought to rely primarily on glycolysis for energy, recent findings have implicated mitochondria in the regulation of stem cell fate and function, particularly in the context of aging and disease.[8–11] A notable example is hematopoietic stem cells (HSCs), in which mitochondria are distributed unevenly during cellular division. This asymmetric distribution appears to be linked to the "stemness" and potency of daughter cells.[12,13] Moreover, HSCs from young and old mice have been observed to exhibit differences in mitochondrial potential and

Address correspondence: Liangyi Chen, New Cornerstone Science Laboratory, National Biomedical Imaging Center, State Key Laboratory of Membrane Biology, Beijing Key Laboratory of Cardiometabolic Molecular Medicine, Institute of Molecular Medicine, School of Future Technology, Center for Life Sciences, Peking University, Beijing 100871, China. E-mail address: lychen@pku.edu.cn (L. Chen); Riguo Fang, EdiGene Inc., Beijing, China. E-mail address: rgfang@edigene.com (R. Fang); Gang Huang, Departments of Cell Systems and Anatomy/Pathology and Laboratory Medicine, UT Health San Antonio, Joe R. and Teresa Lozano Long School of Medicine, 8403 Floyd Curl Drive, San Antonio, TX 78229. E-mail address: huangg1@uthscsa.edu (G. Huang).

Conflict of interest: The authors declare that they have no conflict of interest.

Z.S. and X.Z. contributed equally to this work.

The source code for the bioinformatic pipeline is publicly available at https://github.com/tornado2047/HSC-pipeline.

The raw sequence data reported in this paper have been deposited in the Genome Sequence Archive/Genomics Proteomics & Bioinformatics 2021) in the National Genomics Data Center (Nucleic Acids Res 2022), China National Center for Bioinformation/Beijing Institute of Genomics, Chinese Academy of Sciences (GSA: CRA015596) that are publicly accessible at https://ngdc.cncb.ac.cn/gsa. Image data are available in the BioImage Archive (https://www.ebi.ac.uk/bioimage-archive) under accession number S-BIAD1095.

Blood Science (2025) 7, 1–7:e00236.

Received July 17, 2024; Accepted April 15, 2025.

http://dx.doi.org/10.1097/BS9.0000000000000236

antioxidant interventions, which reduce mitochondrial reactive oxygen species (ROS) production and enhance the function of aged HSCs.[14,15] Despite these insights, the precise effects of aging on the structure and morphology of mitochondria in live HSCs remain incompletely understood. Similarly, the specific mechanisms by which mitochondrial impairment leads to aging or senescence in HSCs are yet clearly defined.

Investigating mitochondria within live HSCs poses challenges due to the small size of these cells, often below the resolving power of conventional fluorescence microscopy for discerning detailed mitochondrial morphologies. Although super-resolution (SR) microscopy techniques overcome the diffraction limit to achieve a higher resolution, they typically require photon flux levels potentially harmful to live-cell SR imaging.[16,17] Moreover, mitochondria are particularly susceptible to phototoxic effects and damage under the intense illumination required for SR imaging in live-cell context.[18] These obstacles impede the visualization and quantification of mitochondrial dynamics in live HSC. Beyond imaging limitations, live-cell imaging techniques inherently lack the capacity to provide comprehensive molecular information. Single-cell RNA sequencing (scRNA-seq) offers detailed molecular profiles,[19] but it is limited to capturing static snapshots from fixed cell populations. This approach complicates efforts to extract the temporal and dynamic aspects of biological processes. Integrating spatial omics with multiplexed imaging technologies enables a more complete understanding of molecular profiles and their spatial heterogeneity within cells and their microenvironments.[20] However, linking these molecular profiles to the varying states of organelles within cells remains an unresolved challenge.

In this study, differences in mitochondrial and transcriptome profiles were explored between HSCs isolated from young and aged mice, with the latter group exhibiting diminished stemness features. Spinning-disc structured illumination microscopy (SD-SIM) combined with a sparse deconvolution algorithm was employed to enable 3-dimensional SR imaging of mitochondria with reduced phototoxicity.[21] This approach facilitated the meaningful categorization of single-cell transcriptome data obtained subsequently from the same cells. A comprehensive open-source pipeline is proposed, integrating differential gene expression analysis and gene regulatory networks with a trajectory-informed reference for mitochondrial morphological transformations. A set of genes potentially critical in directing alterations to HSCs fate was identified. Among the GDF15 emerged as a key factor linking mitochondrial morphology with HSCs potency and aging. This finding highlights the effectiveness of the proposed methodological framework in elucidating complex interactions between cellular structures and gene function.

2. MATERIALS AND METHODS

2.1. Mice

Experiments were conducted using young (6–8-week-old) and aged (12–22-month-old) female C57BL/6J mice obtained from Charles River. The mice were housed under improved hygienic conditions in individually ventilated cages, with 2 to 5 mice per cage, and provided with environmental enrichment. Housing conditions included an inverse 12-hour day–night cycle in a temperature (21 ± 2°C) and humidity (55 ± 10%) controlled room, with ad libitum access to standard diet and drinking water. All experiments and animal care procedures were approved by the Lund University Animal Ethics Committee.

2.2. Long-term HSC isolation by FACS sorting

Murine bone marrow cells were isolated from the femora and tibiae of female C57/BL6J mouse by flushing the bones with phosphate-buffered saline (PBS) supplemented with 1% human serum albumin (HSA). The cells were filtered through a 40 µm cell strainer, centrifuged, and the pellet was resuspended in red blood cells (RBC) lysis buffer (Biolegend, San Diego, California, 420301) for 10 minutes. Following RBC lysis, the cells were incubated with an anti-CD16/32 (Biolegend, 101301) antibody for 10 minutes to block Fc receptors. Staining for long-term HSCs was performed using the following anti-mouse antibodies: lineage fluorescein 5-isothiocyanate (FITC)-conjugated antibodies specific for CD11b (Biolegend,101205), CD3 (Biolegend,100203), Gr1 (Biolegend,108405), CD45R (Biolegend,103205), and Ter119 (Biolegend,116205), PE-conjugated CD117/c-kit (Biolegend,105807), BV421-conjugated Ly-6A/E/Sca-1 (Biolegend,108127), BV510-conjugated CD150 (Biolegend,115929), APC-conjugated CD48 (Biolegend,103411), and 7-AAD (Biolegend,420404) for viability assessment. Cells were stained for 15 minutes in the dark, washed with PBS, and centrifuged. The cell pellets were resuspended in PBS, and LT-HSCs (LSK/SLAM) were isolated using a Beckman Coulter Astrios EQ high-speed cell sorter.

2.3. LT-HSC culture and GDF15 antibody treatment in vitro

Cell culture plates (Cellvis, Mountain View, California, D35-10-1-N) were coated with 100 µg/mL fibronectin (Gibco: Life Technologies Corporation, Grand Island, New York, PHE0023) for 24 hours before cell sorting. LT-HSCs were sorted directly into the serum-free StemSpan™ SFEM (StemCell Technologies: STEMCELL Technologies Canada Inc., Vancouver, British Columbia, Canada, 09600) supplemented with 10 ng/mL murine interleukin-6 (IL6; PeproTech, Cranbury, New Jersey, 216-16-10), 10 ng/mL murine stem cell factor (SCF; PeproTech, 250-03-10), 100 ng/mL murine thrombopoietin (TPO; PeproTech, 315-14-50), 30 ng/mL murine Fms-related tyrosine kinase 3 ligand (Flt-3L, R&D, 427-FL-005), and 100 U/mL penicillin, and 100 µg/mL streptomycin (Gibco, 15140122). LT-HSCs were cultured in a complete medium at 5% O_2 and 37°C for 24 hours. For GDF15 antibody experiments, 20 µg/mL GDF15 antibody (Abcam, Trumpington, United Kingdom, ab242888) or 20 µg/mL isotype (Abcam, ab210849) was added to the complete medium, and cells were cultured for 24 hours.

2.4. Mitochondria staining

After 24 hours of culture, cells were incubated with MitoTracker Green (MTG, 0.67 µM, dissolved in PBS from an original 100 µM stock solution in dimethyl sulfoxide [DMSO], Cell Signaling Technology, Inc., Danvers, Massachusetts, 9074S) in the presence of verapamil (83 µM, dissolved in PBS from an original 50 mM stock solution in DMSO, Selleck, S4202) at 37°C for 10 to 20 minutes. Cells were then stained with Hoechst (0.6 µg/mL, dissolved in PBS from an original 10 mg/mL stock solution in DMSO; Sigma, B2261) at 37°C for 5 to 8 minutes, followed by washing with 1× PBS.

2.5. Mitochondria imaging with SD-SIM and data analysis

After staining, LT-HSCs were imaged for mitochondrial and nuclear visualization. SD-SIM was performed using the live-SR module (GATACA system), on an inverted fluorescence microscope (IX83, Olympus, Tokyo, Japan) equipped with a scanning disk confocal system (Yokogawa, Tokyo, Japan, CSU-X1). All experiments used a 1.30 numerical aperture (NA) oil objective lens (100×) and 2 laser beams (405 and 488 nm). Images were acquired using an EMCCD (Andor Technology [Oxford Instruments Andor], Belfast, Northern Ireland, United Kingdom, iXon3 897) and sCMOS (Hamamatsu Photonics, Hamamatsu, Shizuoka, Japan, c14440-20up). All images were captured using the ImageJ software and sparsely deconvolved using commercial

software (MicroscopeX FINER, CSR Biotech, Guangzhou, China).

2.6. Colony-forming unit assays of GDF15-treated LT-HSC from old mice

As previously described (Caroline A., 2021), LT-HSCs from aged mice were sorted into StemSpan™ SFEM (StemCell Technologies, 09600) supplemented with 20 ng/mL human IL-11 (PeproTech, 200-11-10UG), 2 mM L-Glutamine (Gibco, 25030081), 100 U/mL penicillin, 100 µg/mL streptomycin (Gibco, 15140122), and 10% fetal blood serum (Gibco, 10100147C) with or without 20 µg/mL GDF15 antibody. The culture of LT-HSCs was carried out in a medium containing 5% O_2 at 37°C for 7 days. Cultured cells were transferred from liquid medium to MethoCult M3434 (Stem Cell, 03434) and cultured for 14 days. Colony types were scored by antibody staining with FITC-conjugated CD41 (BioLegend, 133903), APC-conjugated Gr-1 (BioLegend, 108412), PE/Cyanine7-conjugated Ter-119 (BioLegend, 116222), and PE-conjugated CD11b (BioLegend, 101207). Samples were acquired on a Novocyte 2060R (ACEA), and flow cytometry data were analyzed using FlowJo.

2.7. Method of quantifying mitochondrial morphology patterns

Categorical variables "short-dispersed (SD)," "long-dispersed (LD)," and "long-polarized (LP)" were assigned values of 1, 0.5, and 0, respectively. Each cell was then associated with a mitochondrial morphology score (F). Within the UMAP plot, the k-nearest neighboring cells to each cell were identified (using the Euclidean distance metric, where $k = 5$). Subsequently, the average F value among these k +1 cells was calculated as a quantitative measure of the mitochondrial morphology patterns.

3. RESULTS

Since the regenerative capabilities of mice diminish with age, HSCs from young and aged mice were used to benchmark differences between high- and low-quality stem cells. Bone marrow cells were first flushed and labeled with fluorescent antibodies before using a FACS machine to sort long-term HSCs (LT-HSCs), which were characterized as lineage-negative, c-Kit-positive, Sca1-positive, CD150-positive, and CD48-negative (LSK-SLAM) (Supplementary Figure 1, https://links.lww.com/BS/A117). Subsequently, the cells were labeled with MitoTracker Green in the presence of verapamil to prevent dye efflux, and Hoechst staining was applied to delineate the nuclei. The cells were then visualized using SD-SIM followed by sparse deconvolution (**Fig. 1A**).

SR microscopy revealed considerable heterogeneity in the mitochondria of LT-HSCs. Some LT-HSCs exhibited short mitochondria evenly distributed throughout the cell, while others contained elongated mitochondria either dispersed throughout the cell or arranged polarly relative to the nucleus (**Fig. 1B**). Based on these observations, we categorized mitochondria into 3 phenotypic patterns: SD, LD, and LP. LT-HSCs from both young and aged mice displayed 3 mitochondrial configurations, with a similar frequency of LD phenotype. However, young LT-HSCs showed a higher prevalence of the SD configuration compared to the LP configuration, whereas the reverse was observed in aged LT-HSCs (**Fig. 1B and C**). This suggests that LP and SD mitochondrial configurations may indicate lower and higher stem cell potency, respectively.

Following SR imaging, 217 HSCs were selected using a manipulator under a microscope, lysed, and sequenced. Data analysis was performed using the Seurat (V4) package in R software[22] for batch normalization and dimensional reduction via principal component analysis (PCA). Uniform Manifold Approximation and Projection (UMAP) was then applied to visualize high-dimensional transcriptomic data in two dimensions. From a bioinformatics perspective, the data could be categorized into 2, 3, 5, or 6 distinct clusters depending on resolution parameters (Supplementary Figure 2A, https://links.lww.com/BS/A118). The varying cluster number risked underfitting or overfitting prior biological context. Notably, integrating phenotypic details, such as age and mitochondrial morphology into the genetically informed, dimensionally reduced UMAP revealed that a delineation into 5 clusters provided the most physiologically relevant classification (**Fig. 1E**). Aged mice exhibited a marked overlap with transcriptome cluster 0, while young mice predominantly corresponded with the remaining 4 clusters (Supplementary Figure 2B, https://links.lww.com/BS/A118).

Once the optimal cluster division was determined, a heatmap was generated to display differentially expressed genes (DEGs), aiming to identify potential biomarkers indicative of disparate cell clusters (**Fig. 1D**). Analysis of these biomarkers revealed a close relationship between clusters 0 and 2, while cluster 1 showed a notable resemblance to cluster 4. Advanced pseudo-temporal analysis[23] revealed a progressive shift in the transcriptome states of HSCs following the sequence 3-1-4-2-0 (**Fig. 1F**). This progression corresponded to a gradual transition in mitochondrial morphology from the SD to the LP configuration as HSCs moved from stage 3 to 0 (**Fig. 1G**).

Genes driving transitions between distinct cell states marked by significant shifts in average logarithmic fold change (logFC) were identified (**Fig. 2A**). Since the expression of these marker genes may be regulated by distinct sets of transcription factors, a regulon analysis was performed using the R package SCENIC.[24] The results revealed cluster-specific suggesting a role in mediating state transitions (**Fig. 2B**, Supplementary Figure 2C, https://links.lww.com/BS/A118). By tracking genes influenced by key regulators associated with cell state transitions, a subset of target genes emerged as potential drivers of these dynamics, including clusterin (CLU), immediate early response 3 (IER3), ubiquitin C (UBC), bone morphogenetic protein 4 (BMP4), and growth differentiation factor 15 (GDF15) (**Fig. 2C**). These genes are regulated by the transcription factors JUN and JUNB (Supplementary Figure 2D, https://links.lww.com/BS/A118).

Among these candidates, GDF15 stood out as a particularly strong regulator due to its significantly lower expression in SD cells compared to LD and LP cell types (**Fig. 2D**). GDF15 is highly induced during mitochondrial dysfunction[25] and has been implicated in mitochondrial regulation[26] and human aging.[27] The variable expression of GDF15 in different LT-HSCs types across the pseudotime aligned with the previously described mitochondrial morphological transition from SD to LP (**Fig. 2E**, Supplementary Figure 2E, https://links.lww.com/BS/A118).

GDF15 is known to influence mitochondrial dysfunction by affecting mitochondrial fission.[28,29] In young LT-HSCs classified within cluster 3, low expression of GDF15 coincided with low expression of the mitochondrial fission-associated genes dynamin 1-like (DNM1L) and mitochondrial fission factor (MFF) (**Fig. 2F**). As cells progressed from cluster 1 to cluster 0, a shift that signaled increased cellular senescence, there was a gradual upregulation of GDF15 expression. Conversely, DNM1L and MFF expression levels initially increased but subsequently decreased (**Fig. 2F**). This pattern suggests an inverse relationship between GDF15 and mitochondrial fission processes, linking elevated GDF15 expression with alterations in mitochondrial distribution and HSC aging.

GDF15 is secreted extracellularly and binds to GFRAL receptors on the plasma membrane to exert its effects.[30] To investigate its role, LT-HSCs from aged mice were treated with a GDF15-specific neutralizing antibody, with a mock solution and isotype antibody used as controls. Although LT-HSCs exposed to the mock solution and isotype antibody retained elongated mitochondrial structures, those treated with the GDF15-specific antibody exhibited a transition toward a more fragmented and

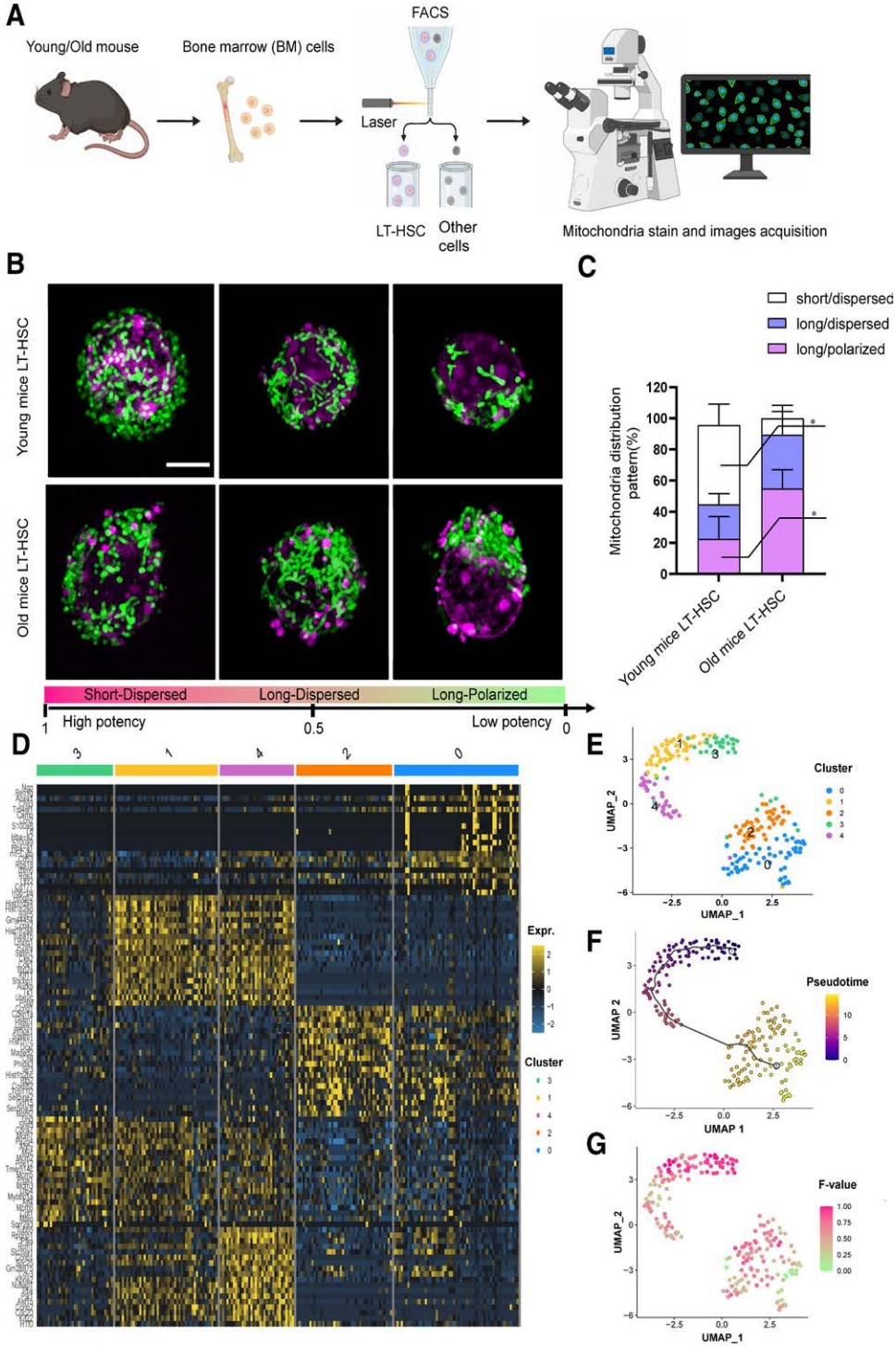

Figure 1. Mitochondria morphology assisted the clustering of scRNA-seq data from young and aged LT-HSCs. (A) A schematic diagram of the process for isolating and imaging LT-HSCs from both young and old mice. (B) Mitochondria imaging results from young and aged mice LT-HSCs under the SR microscopy, categorized into 3 patterns of distribution: SD, LD, and LP. The likelihood of cellular differentiation potency is highest in the SD configuration (indicated by the pink bar), whereas it is lowest in the LP configuration (represented by the green bar). A quantitative score is attributed to each pattern: 1 for SD, 0.5 for LD, and 0 for LP. (C) The percentage of mitochondria distribution pattern between young (n = 99) and old LT-HSCs (n = 64). Unpaired *t* test: **p* < 0.05. (D) A 2D UMAP plot displaying Louvain clustering from Seurat applied to the entire dataset of 217 cells. (E) A heatmap shows gene expression profiling of the top 20 distinct genes within each cluster. The differential genes identified for each cluster are listed in Table S1, https://links.lww.com/BS/A120. (F) Pseudotime trajectory analysis of the 217 cells performed with Monocle3 reveals the likely progression of cellular states along the sequence from cluster 3 through clusters 1, 4, 2, to cluster 0. (G) Visualization of quantified mitochondrial morphology patterns superimposed on the UMAP plot. LD = long/dispersed, LP = long/polarized, LT-HSC = long-term hematopoietic stem cell, scRNA-seq = single-cell RNA sequencing, SD = short/dispersed, SR = super-resolution, UMAP = Uniform Manifold Approximation and Projection.

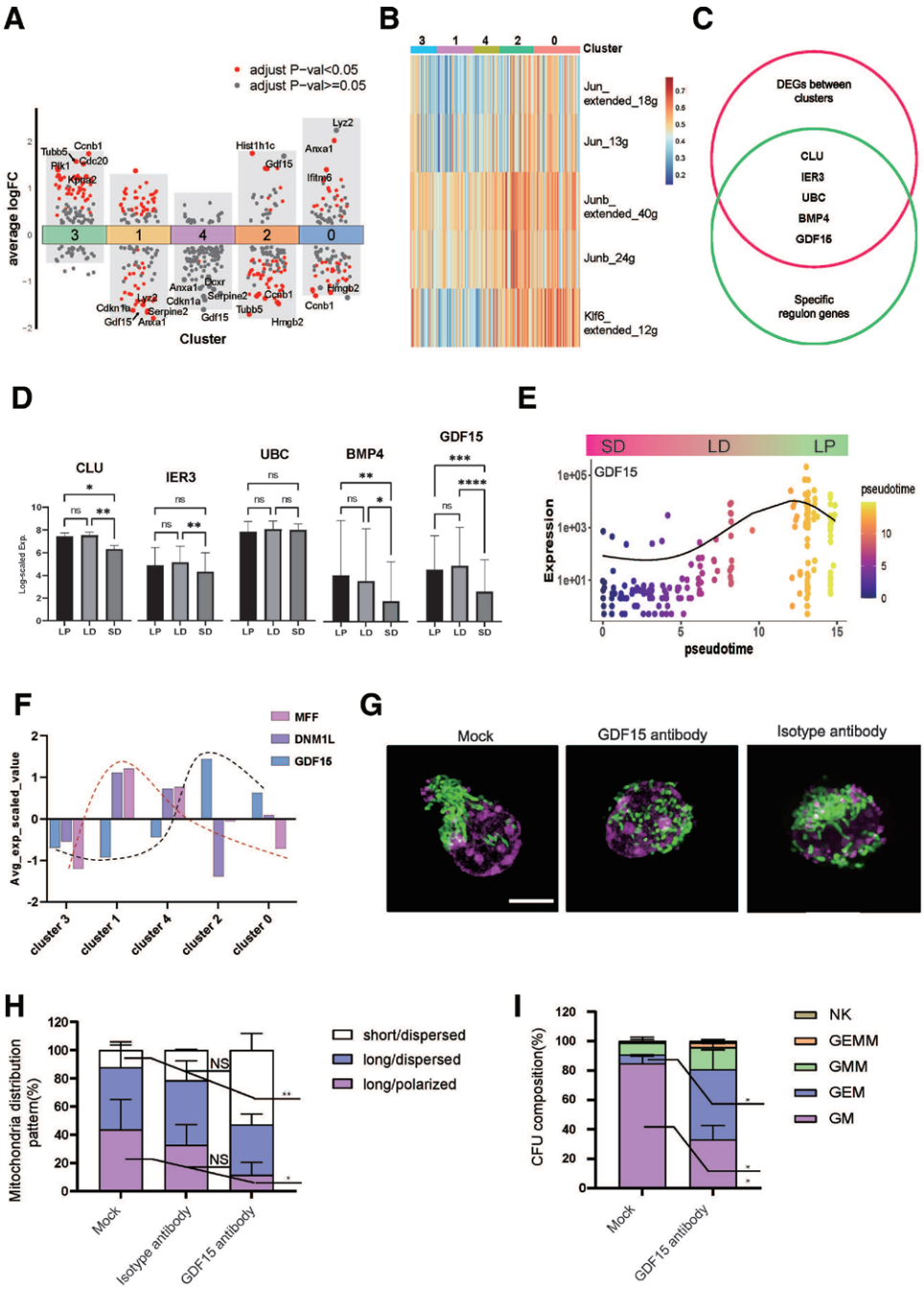

Figure 2. The integration of SR imaging with scRNA analysis pipeline reveals the critical role of GDF15 in aging LT-HSCs. (A) Volcano plots illustrate the DEGs across the 5 identified clusters. (B) The heatmap depicts the activity changes of specific regulons across different clusters. (C) A Venn diagram highlights the common DEGs shared between clusters and key transcriptional regulatory genes, among which are CLU, IER3, UBC, BMP4, and notably GDF15. (D) Log-scaled expression level of target genes in LP, LD, and SD cells, GDF15 is the most significant marker. Unpaired *t* test: **p* < 0.05, ***p* < 0.01, ****p* < 0.001. (E) A plot traces the expression variations of GDF15 across LP, LD, and SD cellular states over pseudotime. (F) The histograms show the relative expression of GDF15 and mitochondrial fission-associated genes (DNM1L and MFF) in different clusters. (G) Representative images of mitochondria from aged LT-HSCs in untreated (Mock), treated (GDF15 antibody), and control groups (Isotype antibody). (H) The percentage of mitochondria distribution pattern in untreated (Mock) (n = 111), isotype antibody-treated (n = 64), and GDF15 antibody-treated aged LT-HSCs (n = 209). Unpaired *t* test: **p* < 0.05, ***p* < 0.01. (I) Colony subtype analysis shows that the majority of cells (~67%) generated colonies of at least 3 lineages after GDF15 antibody treatments in CFU assays. Conversely, the majority of cells (~85%) only generate colonies of 2 lineages without GDF15 antibody treatments (Mock, n = 99, 3 repeats; GDF15 antibody, n = 92, 3 repeats). Colonies are defined as MK (containing cells positive for megakaryocyte marker CD41), GM (containing cells positive for granulocyte/monocyte markers Gr1 and CD11b), GEM (positive for GM and erythrocyte markers Gr1, CD11b, and Ter-119), GMM (positive for GM and MK markers), and GEMM (positive for GM, MK, and E markers), as described in the experimental procedures. Bars show the mean with SEM. Unpaired *t* test: **p* < 0.05. CFU = colony-forming unit, DEG = differentially expressed gene, GDF15 = growth differentiation factor 15, LD = long/dispersed, LP = long/polarized, LT-HSC = long-term hematopoietic stem cell, SD = short/dispersed, SEM = standard error of the mean, SR = super-resolution.

dispersed mitochondrial morphology, resembling the mitochondrial profile of LT-HSCs from young mice (**Fig. 2G and H**). The stemness of treated LT-HSCs was subsequently assessed using a colony-forming unit (CFU) assay.[31] In the mock-treated group, a majority (75%–90%) of the LT-HSCs differentiated into only 2 lineages, identified by the granulocyte/monocyte markers Gr1

and CD11b (GM). This subset of cells was reduced by 20% to 40% in the group treated with the GDF15 antibody (**Fig. 2I**). In contrast, 60% to 70% of single LT-HSCs treated with the GDF15 antibody differentiated into at least 3 distinct lineages (cells positive for GM and erythrocyte markers Gr1, CD11b, and Ter-119, GEM; cells positive for GM and megakaryocyte marker CD41, GMM). Conversely, only 10% to 15% of single LT-HSCs in the mock group produced 3 lineage types, with no instances of colony formation encompassing 4 lineages (cells positive for GM, MK, and E markers, GEMM) (**Fig. 2I**). These results suggest that GDF15 plays a causative role in regulating mitochondrial distribution and maintaining stemness in LT-HSCs.

4. DISCUSSION

Recently advances have seen a growing number of study combining high-content imaging with multiomics analysis to establish connections between morphological characteristics, molecular profiles, and genetic modifications.[32,33] For example, RNA expression profiles have been predicted using Raman microscopy,[34] and systematic labeling of endogenous proteins has been employed to derive general principles of cellular organization.[35] Furthermore, by correlating the subcellular localization of proteins in segregating cells viewed through immunofluorescence microscopy with scRNA-seq data, significant cell-to-cell variability during the cell cycle has been revealed.[36] Despite these breakthroughs, acquiring subcellular images with resolution and contrast remains a persistent challenge in such studies. Consequently, discerning the physiological significance of numerous features whether manually curated[33] or generated through deep learning approaches such as autoencoders[35]—remains difficult. Additionally, researchers often need to collect and curate vast image datasets, sometimes extending to hundreds of thousands, to accurately correlate them with genomic and proteomic data. This represents a significant effort and poses challenges for most researchers.[37] In this study, 2 significant benefits of integrating SR imaging with transcriptomic profile analysis were highlighted. First, the improved resolution and contrast provided by SR imaging facilitate the precise identification and analysis of subcellular structures, such as mitochondria. Even the basic features of these organelles were sufficient to enable meaningful categorization of transcriptional data extracted from a modest sample of 200 single cells. Second, by leveraging mitochondrial morphological changes as prior knowledge, a systematic approach was employed to filter variable transcripts and identify 5 key genes, with one in particular linking aging and mitochondrial function. In addition, differential expression (DE) analysis, trajectory inference (TI), and gene regulatory network (GRN) analysis were integrated to uncover critical genes involved in cell state transition. The open-source pipeline consists of 2 primary modules: the first utilizes Seurat and SCENIC to identify characteristic DEGs, while the second applies Monocle3 to detect markers exhibiting expression patterns aligned with those observed in the initial step and during morphological changes (Supplementary Figure 3, https://links.lww.com/BS/A119). Thus, combining SR imaging with this analytical pipeline offers a straightforward and powerful approach for extracting essential information from limited biological samples.

The identification of GDF15 as a candidate target inversely associated with HSCs stemness aligns with the close relationship between the stemness of HSCs and mitochondria.[38,39] Diseases such as tumors and metabolic disorders are known to influence mitochondrial dynamics, leading to GDF15 overexpression.[40,41] In contrast to these studies, the findings here emphasize that intrinsic upregulation of GDF15 may cause mitochondrial elongation, possibly by orchestrating the interplay between the GDF15 complex[30] and DRP1 molecules.[29] Therefore, GDF15 may act as a critical node in circularly linking mitochondrial morphology and function with stemness in HSCs, which could serve as a target for manipulation in diverse physiological contexts ranging from HSCs stemness and metabolic disorders to other age-related processes.

In summary, we propose that combining SR imaging with a bioinformatics pipeline provides a highly efficient method for identifying key molecules involved in cellular and subcellular morphological changes and cell stage transitions, even with a small dataset. This approach holds broad potential for applications and translational impact, establishing it as a highly relevant methodology.

ETHICAL APPROVAL

All procedures were carried out in accordance with the guidelines and regulations of the animal ethics committee of Peking University. The study protocol was reviewed and approved by the animal ethics committee of Peking University (approval number: IMM-ChenLY-1). Efforts were made to minimize the number of animals used and to ensure their well-being throughout the study.

REFERENCES

[1] Akbari M, Kirkwood TBL, Bohr VA. Mitochondria in the signaling pathways that control longevity and health span. *Ageing Res Rev* 2019;54:100940.

[2] Luo Y, Ma J, Lu W. The significance of mitochondrial dysfunction in cancer. *Int J Mol Sci* 2020;21:5598.

[3] Zhou Z, Austin GL, Young LEA, Johnson LA, Sun R. Mitochondrial metabolism in major neurological diseases. *Cells* 2018;7:229.

[4] Prasun P. Mitochondrial dysfunction in metabolic syndrome. *Biochim Biophys Acta Mol Basis Dis* 2020;1866:165838.

[5] Amorim JA, Coppotelli G, Rolo AP, Palmeira CM, Ross JM, Sinclair DA. Mitochondrial and metabolic dysfunction in ageing and age-related diseases. *Nat Rev Endocrinol* 2022;18:243–258.

[6] Sharpe A, McKenzie M. Mitochondrial fatty acid oxidation disorders associated with short-chain enoyl-CoA hydratase (ECHS1) deficiency. *Cells* 2018;7:46.

[7] Rafalski VA, Mancini E, Brunet A. Energy metabolism and energy-sensing pathways in mammalian embryonic and adult stem cell fate. *J Cell Sci* 2012;125:5597–5608.

[8] Ansó E, Weinberg SE, Diebold LP, et al. The mitochondrial respiratory chain is essential for haematopoietic stem cell function. *Nat Cell Biol* 2017;19:614–625.

[9] Bao F, Zhou L, Zhou R, et al. Mitolysosome exocytosis, a mitophagy-independent mitochondrial quality control in flunarizine-induced parkinsonism-like symptoms. *Sci Adv* 2022;8:eabk2376.

[10] Khacho M, Clark A, Svoboda DS, et al. Mitochondrial dynamics impacts stem cell identity and fate decisions by regulating a nuclear transcriptional program. *Cell Stem Cell* 2016;19:232–247.

[11] Zhang H, Ryu D, Wu Y, et al. NAD $^+$ repletion improves mitochondrial and stem cell function and enhances life span in mice. *Science* 2016;352:1436–1443.

[12] Katajisto P, Döhla J, Chaffer CL, et al. Asymmetric apportioning of aged mitochondria between daughter cells is required for stemness. *Science* 2015;348:340–343.

[13] Hinge A, He J, Bartram J, et al. Asymmetrically segregated mitochondria provide cellular memory of hematopoietic stem cell replicative history and drive HSC attrition. *Cell Stem Cell* 2020;26:420–430.e6.

[14] Mohrin M. Mito–managing ROS & redox to reboot the immune system: tapping mitochondria & redox management to extend the reach of hematopoietic stem cell transplantation. *Free Radic Biol Med* 2021;165:38–53.

[15] Morganti C, Ito K. Mitochondrial contributions to hematopoietic stem cell aging. *Int J Mol Sci* 2021;22:11117.

[16] Schermelleh L, Ferrand A, Huser T, et al. Super-resolution microscopy demystified. *Nat Cell Biol* 2019;21:72–84.

[17] Godin AG, Lounis B, Cognet L. Super-resolution microscopy approaches for live cell imaging. *Biophys J* 2014;107:1777–1784.

[18] Yang Z, Li L, Ling J, et al. Cyclooctatetraene-conjugated cyanine mitochondrial probes minimize phototoxicity in fluorescence and nanoscopic imaging. *Chem Sci* 2020;11:8506–8516.

[19] Nguyen A, Khoo WH, Moran I, Croucher PI, Phan TG. Single cell RNA sequencing of rare immune cell populations. *Front Immunol* 2018;9:1553.

[20] Lewis SM, Asselin-Labat M-L, Nguyen Q, et al. Spatial omics and multiplexed imaging to explore cancer biology. *Nat Methods* 2021;18:997–1012.
[21] Zhao W, Zhao S, Li L, et al. Sparse deconvolution improves the resolution of live-cell super-resolution fluorescence microscopy. *Nat Biotechnol* 2022;40:606–617.
[22] Hao Y, Hao S, Andersen-Nissen E, et al. Integrated analysis of multimodal single-cell data. *Cell* 2021;184:3573–3587.e29.
[23] Cao J, Zhou W, Steemers F, Trapnell C, Shendure J. Sci-fate characterizes the dynamics of gene expression in single cells. *Nat Biotechnol* 2020;38:980–988.
[24] Aibar S, González-Blas CB, Moerman T, et al. SCENIC: single-cell regulatory network inference and clustering. *Nat Methods* 2017;14:1083–1086.
[25] Wang D, Day EA, Townsend LK, Djordjevic D, Jørgensen SB, Steinberg GR. GDF15: emerging biology and therapeutic applications for obesity and cardiometabolic disease. *Nat Rev Endocrinol* 2021;17:592–607.
[26] Liu H, Liu J, Si L, Guo C, Liu W, Liu Y. GDF-15 promotes mitochondrial function and proliferation in neuronal HT22 cells. *J Cell Biochem* 2019;120:10530–10547.
[27] Conte M, Giuliani C, Chiariello A, Iannuzzi V, Franceschi C, Salvioli S. GDF15, an emerging key player in human aging. *Ageing Res Rev* 2022;75:101569.
[28] Wedel S, Martic I, Guerrero Navarro L, et al. Depletion of growth differentiation factor 15 (GDF15) leads to mitochondrial dysfunction and premature senescence in human dermal fibroblasts. *Aging Cell* 2022;22:e13752.
[29] Yasuda T, Ishihara T, Ichimura A, Ishihara N. Mitochondrial dynamics define muscle fiber type by modulating cellular metabolic pathways. *Cell Rep* 2023;42:112434.
[30] Rochette L, Zeller M, Cottin Y, Vergely C. Insights into mechanisms of GDF15 and receptor GFRAL: therapeutic targets. *Trends Endocrinol Metab* 2020;31:939–951.
[31] Oedekoven CA, Belmonte M, Bode D, et al. Hematopoietic stem cells retain functional potential and molecular identity in hibernation cultures. *Stem Cell Rep* 2021;16:1614–1628.
[32] Haghighi M, Caicedo JC, Cimini BA, Carpenter AE, Singh S. High-dimensional gene expression and morphology profiles of cells across 28,000 genetic and chemical perturbations. *Nat Methods* 2022;19:1550–1557.
[33] Carpenter AE, Jones TR, Lamprecht MR, et al. CellProfiler: image analysis software for identifying and quantifying cell phenotypes. *Genome Biol* 2006;7:R100.
[34] Kobayashi-Kirschvink KJ, Comiter CS, Gaddam S, et al. Prediction of single-cell RNA expression profiles in live cells by Raman microscopy with Raman2RNA. *Nat Biotechnol* 2024;42:1726–1734.
[35] Cho NH, Cheveralls KC, Brunner A-D, et al. OpenCell: proteome-scale endogenous tagging enables the cartography of human cellular organization. *Science* 2022;375:eabi6983.
[36] Mahdessian D, Cesnik AJ, Gnann C, et al. Spatiotemporal dissection of the cell cycle with single-cell proteogenomics. *Nature* 2021;590:649–654.
[37] Hériché J-K, Alexander S, Ellenberg J. Integrating imaging and omics: computational methods and challenges. *Ann Rev Biomed Data Sci* 2019;2:175–197.
[38] Mansell E, Sigurdsson V, Deltcheva E, et al. Mitochondrial potentiation ameliorates age-related heterogeneity in hematopoietic stem cell function. *Cell Stem Cell* 2021;28:241–256.e6.
[39] Papa L, Djedaini M, Hoffman R. Mitochondrial role in stemness and differentiation of hematopoietic stem cells. *Stem Cells Int* 2019;2019:1–10.
[40] Suriben R, Chen M, Higbee J, et al. Antibody-mediated inhibition of GDF15–GFRAL activity reverses cancer cachexia in mice. *Nat Med* 2020;26:1264–1270.
[41] Wang D, Townsend LK, DesOrmeaux GJ, et al. GDF15 promotes weight loss by enhancing energy expenditure in muscle. *Nature* 2023;619:143–150.